Topics in Catalysis (2023) 66:1391–1405
https://doi.org/10.1007/s11244-023-01823-6

ORIGINAL PAPER

Activity of Nickel Supported Over Nanorod-Shaped Strontium Hydroxyapatite Catalysts in Selective Methanation of CO & CO_2

Prem Kumar Seelam[1,2] · Putrakumar Balla[3] · Rajesh Rajendiran[4] · Balaga Ravi[4] · Challa Prathap[4] · Ulla Lassi[1] · Sungtak Kim[3] · Perupogu Vijayanand[4]

Accepted: 19 April 2023 / Published online: 6 May 2023

Abstract

Nickel modified strontium hydroxyapatite (Ni/Sr-HAP) supported catalysts are studied in selective methanation of CO/CO_2. In this work, a new type of nano rod-shaped strontium hydroxyapatite-based catalysts with two different sizes and aspect ratios were prepared by sol–gel method and in next step, Ni precursor was wet impregnated *i.e.,* denoted as Ni/Sr-HAP and Ni/Sr-HAP(F127). The catalytic tests were performed in CO and CO_2 methanation reactions and evaluated the light-off temperatures curves (225–450 °C) under ambient pressure in a fixed-bed flow reactor. The physicochemical properties of the prepared catalysts were characterized by XRD, N_2 physisorption, TEM, SEM, TPR, CO_2/H_2-TPD and H_2-chemisorption techniques. From XRD analysis, both Ni/Sr-HAP and Ni/Sr-HAP(F127) were identified as the hydroxyapatite type structure with high crystallinity and very low intensity peaks corresponds to strontium phosphates as the main phase and structure. The TEM and SEM micrographs of Ni/Sr-HAP catalysts displayed a nano- rod shaped morphology with different dimensions and exhibited average Ni particle size of ~ 9.2 nm. While Ni/Sr-HAP(F127) shown the rod size in the length in the range of 100–250 nm and width in the range of 20–40 nm with average Ni particle size 5.7 nm. The F127 mediated support Sr-HAP synthesis i.e., Ni/Sr-HAP(F127) mesoporous catalyst possessed higher metal surface with smaller Ni particles size and possessed higher CO_2 adsorption capacity. The medium strength basic sites of Ni/Sr-HAP catalyst played an important role in methanation reactions. Based on the characterization and the catalysts activity results, small sized nanorods of Ni/Sr-HAP(F127) is the most active and selective catalyst due to the higher Ni dispersion, higher amounts of medium basic sites, and reducibility character than the bigger nanorods based Ni/Sr-HAP catalyst.

Keywords PtG · SNG · CO_2 · methanation · Ni · Strontium

1 Introduction

The anthropogenic carbon emissions are on rise due to staggering number of human and economic activities [1]. Decarbonizing the whole energy chain is the utmost important strategy at global scale. Reducing carbon emissions is highly critical at this moment due to climate change and air pollution problems. The cleanest form of reducing earth's CO_2 and CO emissions is to produce methane or synthetic natural gas (SNG) and found to be potential green transition technology *i.e.,* power-to-gas (PtG) [2, 3]. Therefore, the methanation of carbon oxides is a key mitigation method and converting abundant carbon emissions into more useful energy in the form of methane gas, which is highly feasible with the existing gas infrastructure. Thus, the concept of PtG technology can be a medium-to-long term solution for the future [3, 4].

✉ Prem Kumar Seelam
prem.seelam@oulu.fi

1 Sustainable Chemistry Research Unit, Faculty of Technology, University of Oulu, P.O. Box 4300, 90014 Oulu, Finland

2 Hycamite TCD Technologies Oy, Kemirantie 15, 67900 Kokkola, Finland

3 Department of Chemical Engineering and Applied Chemistry, Chungnam National University, Daejeon 34134, Republic of Korea

4 Energy and Environmental Engineering Department, CSIR-Indian Institute of Chemical Technology, Hyderabad, Telangana 500007, India

1.1 Catalysts for Methanation of CO/CO_2

State of art on catalysts development in CO/CO_2 methanation was tremendous and exponential growth of research articles was foreseen. Methanation or hydrogenation of CO/CO_2 (Sabatier reaction) is well investigated reaction [5, 6]. And moreover, CO methanation is already matured and industrially commissioned reaction to produce SNG from biomass and coal gasification Boll et al. [7]. Both CO and CO_2 methanation are exothermic reactions and favorable at moderately low temperatures (≤ 400 °C) [7, 8]. Moreover, CO_2 is more stable molecule than CO and the methanation of CO_2 possess big challenge in thermal conversion due to thermodynamic limitations and kinetic barrier [9]. Thus, designing and developing a novel catalytic material is a key issue. Further, CO_2 is a more stable molecule and difficult to break the O = C = O bonds and in addition, CO_2 chemistry and reactivity is different than CO [10, 11]. The metal catalyst and support morphology and the structure had significant effect on the catalytic performance in the various solid materials catalysed reactions. In literature wide range of metal-supported catalysts are employed in CO/CO_2 methanation such as Ni, Ru, Co, Cu, Pt-based catalysts studied over a wide range of support materials such as Al_2O_3, SiO_2, ZnO_2, zeolites, carbon, BaO_2, CeO_2, ZrO_2, La_2O_3, MgO and their combination and also promoters and additives such as Fe, Pt, Pr, Sm, Sr, Bi, alkaline-earth metals (Mg, Ba, Ca, Sr) etc. were studied and used to improve the stability and activity of the catalysts [8, 12-14]. The Ni-based catalysts have been the far most popular active metal studied in both CO & CO_2 methanation reactions due to low cost, high activity, and high CH_4 selectivity [13, 15]. Moreover, the Ni-based catalysts is widely studied due to its maturity at industrial scale than other active phase e.g., Ru and Fe catalysts due to aforementioned advantages. There are numerous studies dedicated to Ni-based supported catalysts and investigated various synthesis parameters such as the effect of Ni synthesis methods, final catalyst composition, promotional effects, bimetallic systems, secondary, and tertiary doped oxides, and mixed metal/alkaline/alkali oxides [8, 14, 16]. Recently, most of the research are concentrated on developing catalyst support materials for the Ni-based catalytic materials. Typically, promoters and additives are introduced to improve the reducibility, CO_2 adsorption capacity, reactivity, and metal dispersion. Example, in Cho et al. [12], CaO with optimal 5 wt.% in Ni/Al_2O_3 catalysts was prepared by one-step melt infiltration and Ca enhanced the CO_2 adsorption and the reducibility of the Ni sites [12]. It is critical to determine the optimal loadings of the base metal Ni and the promoters to have sufficient sites and accessibility and avoiding Ni sintering.

The support acidity and basicity had a pronounced effect on the product formation [13, 14]. Most importantly, the strength, amount, and type of acidity/basicity is crucial in determining the superior reaction performance. Different supports have varied acido-basic properties and its composition is key. For example, alumina (Al_2O_3) is widely studied support materials in methanation reactions in combination with Ni and other supports [8, 13]. As we know, Al_2O_3 possess Lewis acidity and the Ni/Al_2O_3 catalysts typically a positively charged acidity had strong affinity towards $HCOO^-$ charged species and inhibit the CO_2 molecule to convert into CH_4 molecules. Whereas, over Ni/SiO_2 and Ni/H-β40 catalysts possess high amount of medium to strong basic sites than alumina supported catalysts and these basic sites are important in the formation of formate intermediate species which finally converts into CH_4 [17]. The methanation of CO/CO_2 is highly favorable over basic character supported catalysts than strong acidity. The effect of lanthanum loadings (1–7 wt.%) was studied in Ni/La_2O_3/hydroxyapatite (HAP) based catalysts. The La promoted improved the Ni dispersion, basicity, and reducibility character of the catalytic system. The enhanced basic sites is due to the La incorporation, which led to increase the reactivity with CO_2 molecule and possess high thermal stability [18]. The calcium phosphate hydroxyapatite (Ca-HAP) support possesses unique properties such as high thermal stability, tunable acid–base properties, and strong adsorption coefficient with many compounds. The acid–base properties can be changed by varying the Ca/P molar ratio in HAP structure [19-21].

Typically, at low Ca/P ratios in HAP exhibited higher acidity values and at higher ratios *i.e.,* Ca/P > 1.6 exhibited more basicity. The variation in acid–base properties of the catalyst can be tunable by changing the Ca/P ratio and by substituting with other ions such as Ba^{2+}, Sr^{2+}, Mg^{2+}, etc. replacing Ca^{2+} [12, 20]. In one study, strontium modified hydroxyapatite (HAP) exhibited higher basicity than the Ca-HAP in improving the selectivity of acetone in 2-propanol conversion [19, 21]. In Guo et al. [22], studied the effect of alkaline metal doped Ni/SiO_2 catalysts and $Ni/MO/SiO_2$ catalysts where, M = Mg, Ca, Sr, and Ba was prepared by the sequential impregnation method. The SrO doped Ni/SiO_2 catalysts was the best among the studied catalysts and exhibited highly stable compared to other catalysts. In addition, SrO enhanced the activity and inhibits the Ni sintering [22]. However, Ca and other alkaline earth metals doped Ni-based catalysts has been the most popular and widely studied due to abundant, cheap, and easy preparation methods. Furthermore, Sr^{2+} is similar chemistry to that of Ca^{2+} such as same charge density and ionic radii (1.2 Å vs. 1.0 Å) but Sr-HAP is more basic catalysts at high Sr/P ratios [19]. As the Sr to P ratio increases, the density of basic

and acid sites increases linearly. Strontium phosphates in hydroxyapatite structure possess high adsorption capacity due to high basicity and ion exchange sites than Ca-HAP [23]. However, the Sr/P molar ratio is the most important parameter in balancing the acido-basicity sites ratio and in promoting the enhanced activity and selectivity of the reaction. Thus, an optimal Sr/P ratio is of great factor. The Ni modified strontium promoted hydroxyapatite based catalysts is not studied and also the Sr-HAP with different nanorod size and aspect ratios is highly novel. In catalysis, effect of size and active surface area is significant on the reaction performance. Nevertheless, the effect of size and morphology in Ni-based catalytic systems is not explored in methanation reactions. Size and shape controlled synthesis of catalyst support is highly critical to study with Ni-based catalyst. In this work, we introduced F127 surfactant during support synthesis to enhance the physicochemical properties of Sr-HAP support material. The F127 mediated synthesis assisted in better dispersion of the active phase. Incorporation of F127 is well reported in the literature and studied in the materials preparation methods e.g., F127-assisted sol-gel process and moreover, F127 is known for the structure and pore directing agent. The Pluronic F127 solely effects the final morphology, crystallite size, surface area and microporosity of the carrier materials [24]. As reported in Shi et al., 2013, calcination of support-F127 material under elevated temperatures, the polymeric organic template contained composite is readily decomposed and assists in the creation of new porosity to gain high specific area [24]. In this work, it is evident that, Sr-HAP support preparation with F127 addition had increased the surface area and exhibited high pore volume. Thus, F127 assisted Sr-HAP support synthesis in Ni catalyst enhanced the catalytic activity. Further investigations will be carried out to know the stability in long-term test runs. The novelty of the work is to introduce novel synthesis of support materials *i.e.,* Sr-HAP with different modified methods with and without F127 surfactant mediated synthesis in nanorod shaped carriers with different aspect ratios and this is clearly substantiated by structure, morphology, and phase analysis. The synthesised nanorod shaped Sr-HAP supported Ni catalysts with two different sizes were tested in the methanation reactions.

2 Materials and Methods

2.1 Materials

Diammonium hydrogen phosphate [$(NH_4)_2HPO_4$], strontium nitrate [$Sr(NO_3)_2$] and nickel nitrate hexahydrate [$Ni(NO_3)_2{\cdot}6H_2O$] chemicals were procured from Sinopharm Chemical Reagent Co., Ltd and Ammonia solution [NH_4OH] was purchased from Kermel Reagents Co., Ltd.

2.2 Preparation Methods

2.2.1 Preparation of Sr-HAP/Sr-HAP (F127) Supports

In a typical synthesis, 1.58 g of $(NH_4)_2HPO_4$ was dissolved in a 40 mL deionized water. Then, NH_4OH solution was added dropwise under vigorous stirring to reach a final pH of 11. In another beaker 40 mL aqueous solution of containing 4.23 g of $Sr(NO_3)_2$ Sr precursor and prepared according to the studies reported in [24, 25]. In another beaker 40 mL aqueous solution was containing 4.23 g of $Sr(NO_3)_2$ and 2 g of Pluronic co-block polymer F127 was added as a structure directing agent. This solution was added dropwise to the above solution at room temperature. The pH of the mixture was adjusted to 11 by adding NH_4OH solution and stirred for next 30 min. Then it was transferred into a 100 mL Teflon-lined autoclave and sealed. The autoclave was then placed in an electric oven at 160 °C for 12 h. The solid precipitates were collected by filtration and washed with distilled water for several times and dried overnight at 90 °C. Finally, the resultant sample was calcined at 550 °C for 6 h (denoted as Sr-HAP)**.** There are two different samples were prepared one with F127 surfactant (Ni/Sr-HAP(F127) and other one without (Ni/Sr-HAP). Both samples exhibited different surface areas and sizes due to the synthesis procedure.

2.2.2 Preparation of the Ni/Sr-HAP Catalysts

Both Ni/Sr-HAP catalysts were prepared by the impregnation method using an aqueous solution of $Ni(NO_3)_2{\cdot}6H_2O$ as a precursor with Ni nominal loading of ~ 10 wt.%. The as-prepared samples were dried at 120 °C for 12 h and calcined in air at 500 °C for 4 h. The final sample were denoted as Ni/Sr-HAP and Ni/Sr-HAP(F127).

3 Catalyst Characterization

3.1 XRD

The X-ray diffraction (XRD) patterns were recorded on a Rigaku D/Max2500V/PC powder diffractometer with a CuKα radiation source operated at 40 kV with a current of 100 mA. The metal loading was measured by inductively

coupled plasma atomic emission spectroscopy (ICPS-8100 instrument, Shimadzu) with a Plasma-Spec-II spectrometer.

3.2 N_2 Isotherms

Nitrogen sorption measurements were conducted on a Autosorb-1 analyzer (Quanta chrome) at − 196 °C. Prior to the analysis, the samples were degassed at 250 °C for 6 h under vacuum conditions. The specific surface area and pore size distribution were measured using BET (Brunauer–Emmett–Teller) method and BJH (Barret-Joyner-Halenda) method respectively.

3.3 ICP

The metal loading was measured by inductively coupled plasma atomic emission spectroscopy (ICPS-8100 instrument, Shimadzu) with a Plasma-Spec-II spectrometer.

3.4 TEM

The transmission electron microscopy (TEM) images were taken on a Hitachi HT7700 microscope operated at 100 kV. The sample grid was prepared by ultrasonically dispersing the sample in ethanol, depositing droplets of the suspensions onto a carbon-enhanced copper grid, and drying them in air under a lamp. The high-resolution TEM (HRTEM) images were taken on a FEI Tecnai G2 F30 Spirit microscope (300 kV).

3.5 SEM

The scanning electron microscopy (SEM) images were taken on a Philips Fei Quanta 200F instrument operated at 20 kV. The sample was placed on a conductive carbon tape affixed to an aluminum sample holder and coated with Au.

3.6 TPR and TPD

Temperature programmed reduction (TPR) and Temperature programmed desorption (TPD) studies were conducted on an AutoChem 2920 (Micromeritics) instrument with probe molecules. For the TPR experiments 0.05 g of the sample was placed in a U-shaped quartz sample tube. The catalyst was mounted on a quartz wool plug. Prior to the TPR studies, the catalyst sample was pretreated by passing a 30 mL/min N_2 gas flow over it at 200 °C for 1 h. After pretreatment, the sample was cooled to ambient temperature (25 °C) and the TPR analysis was carried out in a 5 vol.% H_2-Ar flow (30 mL/min) while heating from ambient temperature to 700 °C at a rate of 10 °C/min.

4 Catalyst Activity Tests

4.1 CO/CO_2 Methanation Reaction

The CO/CO_2 methanation reactions were carried out in a conventional down flow fixed-bed quartz reactor with an inner diameter of 8 mm under ambient pressure. Approximately, 0.1 g of catalyst was loaded and packed in between the quartz wool of the reactor. The temperature of the reactor was measured using a K-type thermocouple which is in direct contact with the catalyst bed and controlled by a temperature controller connected to the furnace. Prior to the reaction, the catalyst samples were reduced in-situ in a stream of 5 vol.% H_2/Ar at 500 °C for 2 h at ramping rate of 2 °C/min. After cooling down to the reaction temperature (225 °C), a mixture of 20 vol.% CO − 80 vol.% H_2 and 20 vol.% CO_2 − 80 vol.% H_2 gas balanced with Ar flow were introduced at a flow rate of 30 mL.min^{-1}, which is equivalent to the gas hour space velocity (GHSV) of 18,000 mL g^{-1} h^{-1}. The reactor outlet stream was analyzed online by using a gas chromatograph (Agilent 7890A) equipped with a DB-WAX column (60 m length × 0.25 mm diameter × 0.250 µm film thickness) that is connected to a flame ionization detector (FID). The CO/CO_2 conversions and products selectivities (Eqs. 1–6) were calculated according to the following equations.

For CO methanation:

$$\text{CO conversion}\,(X_{CO}) = \frac{[C_{CO2}] + [C_{CH4}]}{[C_{CO}] + [C_{CO2}] + [C_{CH4}]} \times 100 \quad (1)$$

$$\text{CO}_2\ \text{Selectivity}(S_{CO2}) = \frac{[C_{CO2}]}{[C_{CO2}] + [C_{CH4}]} \times 100 \quad (2)$$

$$\text{CH}_4\ \text{Selectivity}(S_{CH4}) = \frac{[C_{CH4}]}{[C_{CO2}] + [C_{CH4}]} \times 100 \quad (3)$$

For CO_2 methanation:

$$\text{CO}_2\ \text{conversion}(X_{CO2}) = \frac{[C_{CO}] + [C_{CH4}]}{[C_{CO}] + [C_{CO2}] + [C_{CH4}]} \times 100 \quad (4)$$

$$\text{CO Selectivity}(S_{CO}) = \frac{[C_{CO}]}{[C_{CO}] + [C_{CH4}]} \times 100 \quad (5)$$

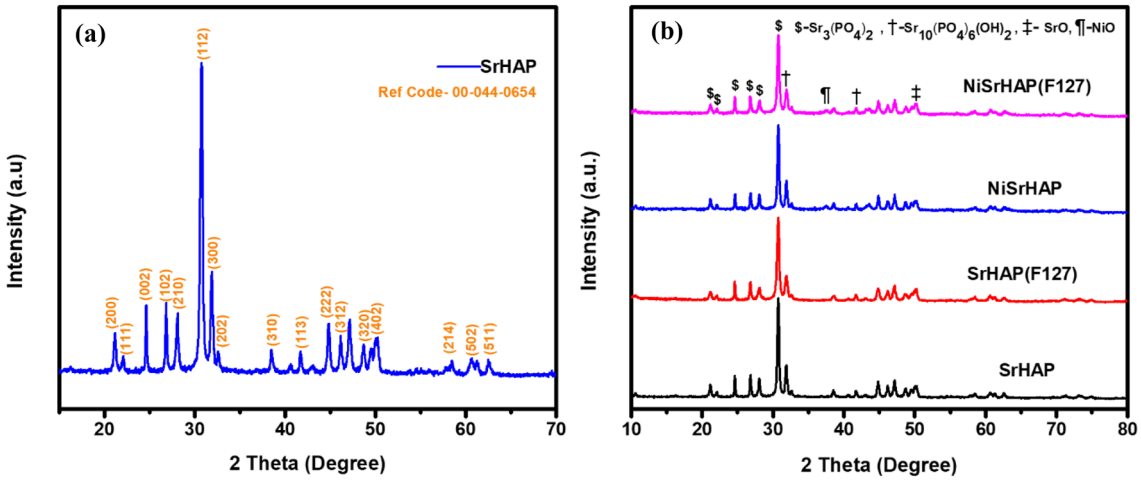

Fig. 1 XRD patterns of **a** as-prepared pure support strontium hydroxyapatite (Sr-HAP) and **b** Sr-HAP & Ni/Sr-HAP catalysts

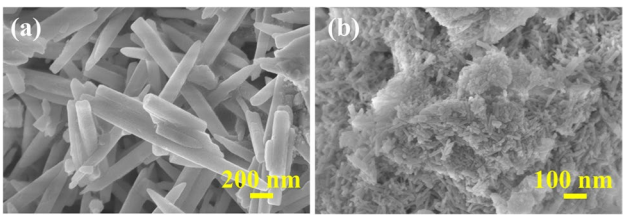

Fig. 2 SEM images of **a** Ni/Sr-HAP and **b** Ni/Sr-HAP(F127) samples

$$\mathrm{CH_4\ Selectivity}\left(\mathrm{S_{CH4}}\right) = \frac{[\mathrm{C_{CH4}}]}{[\mathrm{C_{CO}}] + [\mathrm{C_{CH4}}]} \times 100 \tag{6}$$

where, C_i = *concentration of gases in moles* ($i = CO, CO_2, CH_4$)

$$\text{Carbon balance} = \mathrm{CO} + \mathrm{CO_2} + \mathrm{CH_4} + \mathrm{C} \tag{7}$$

$$\sum_{in}^{mol} mC_{in} = \sum_{out}^{mol} mC_{out}$$

(C_{in} = total moles of carbon input,; C_{out} = total moles of carbon output)

5 Results and Discussion

5.1 XRD Results

The XRD patterns of bare or pure strontium phosphate hydroxyapatite (Sr-HAP) support and the Ni-based strontium hydroxyapatite (Ni/Sr-HAP) materials were displayed in Fig. 1. The Sr-HAP support exhibited sharp peaks with different intensities of a hexagonal crystalline structure belongs to $P6_3m$ crystal group with cell constants $a = b = 9.767$ and $c = 7.265$ [24-26]. The peaks from $2\theta = 10$–$80°$ designated as the strontium hydroxyapatite phases like that of typical calcium-HAP structure and Sr occupy the hexagonal crystal corner similar to Ca [26]. The major phases detected are $Sr_{10}(PO_4)_6(OH)_2$, NiO and minor $Sr_3(PO_4)_2$, SrO phases respectively are well in agreement with previous studies[25-27]. Herein, strontium metal phosphates and corresponding hydrate phases are well depicted with apatite crystals and considered to be the major phases. Few broad peaks from 20 to 25° are assigned to amorphous phase corresponds to Sr-HAP. The NiO diffraction peaks are assigned at $2\theta = 37.2°$, 43° and 62.9° (JCPDS No. 73-2210 & JCPDS No. 47-1049) [12, 26]. These NiO peaks corresponds to (111) and (220) crystal faces and possess relatively imperfect crystallinity. The low intensity diffraction peak at 37.5° is attributed to the NiO phase.

There are no other phases are detected, and it is confirmed and substantiated that the Ni phase is highly dispersed and segregated over the Sr-HAP surface. The Ni and Sr-HAP has distinctive phases, and no mixed phases has been detected (Fig. 1). The Ni/Sr-HAP was prepared in a similar procedure and whereas, in another support preparation was mediated and assisted by F127 surfactant.

5.2 SEM and TEM Results

The scanning micrographs of two catalysts *i.e.,* Ni/Sr-HAP and Ni/Sr-HAP(F127) were presented in Fig. 2a, b. The bigger nanorods shaped morphology of Sr-HAP was clearly visible with high aspect ratio than the powder, slightly amorphous and fragmented into smaller nanorod shaped Sr-HAP(F127) crystals are detected in Fig. 2b. From Fig. 2b, mixed Sr-HAP nano-sized rods of Ni/Sr-HAP(F127) were formed with length 150–250 nm and width in the range of 25–40 nm. The co-block polymer Pluronic F127 was used as a structure directing in modifying the strontium HAP morphology via creation of new porosity. The F127

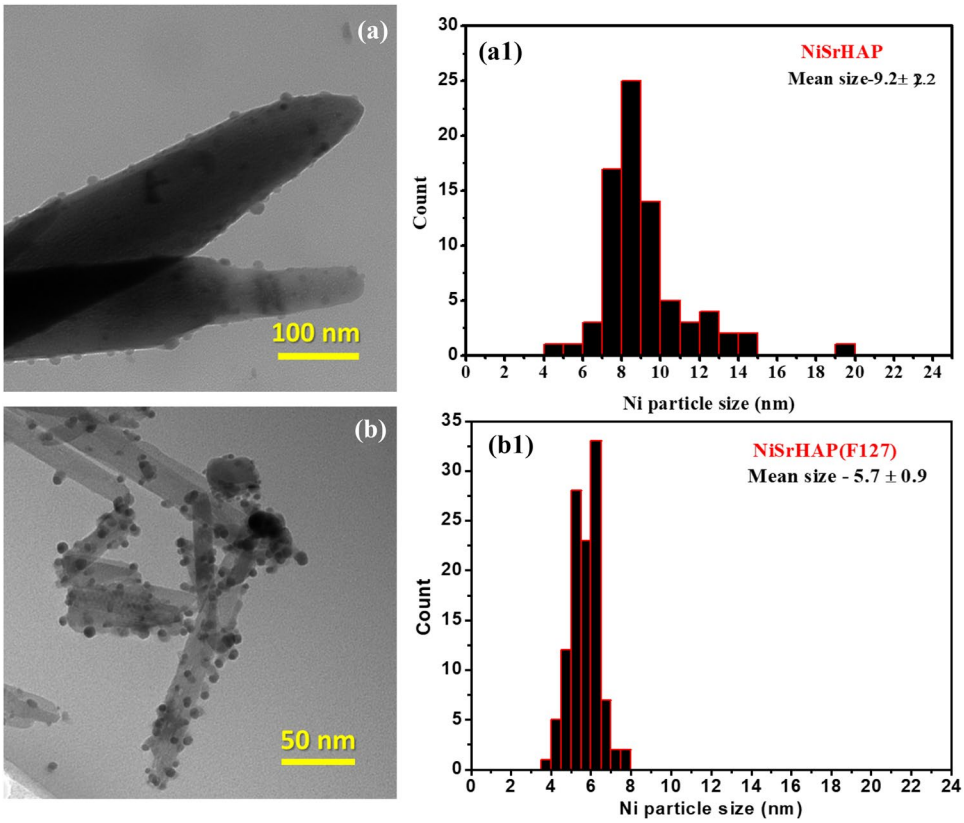

Fig. 3 The TEM images and histograms of Ni nanoparticles and its distribution of the Ni dispersed over nanorods shaped support Sr-HAP samples. **a**, **b** TEM images of Ni/Sr-HAP and Ni/Sr-HAP(F127) samples, **b**, **b1** histograms of Ni particles size distribution

Table 1 Key catalytic properties of the Sr-HAP supports and Ni/Sr-HAP catalysts

Catalyst	Ni[a] (wt.%)	BET surface area[b] (m^2/g)	Average pore size[b] (nm)	Cumulative Pore volume[b] (cc/g)	Ni active surface area[c] (m^2/g_{cat})	Ni Avg. size[c](nm)
Sr-HAP	–	24.4	20.3	0.085	–	–
Ni/Sr-HAP	9.47	21.6	11.3	0.074	6.86	9.3
Sr-HAP(F127)	–	91.7	9.1	0.156	–	–
Ni/Sr-HAP(F127)	9.62	82.2	5.6	0.134	9.68	6.7

[a]ICP analysis
[b]BET analysis
[c]H_2 chemisorption

addition effected the significant reduction in nanorod size from 1200–1600 to 100–250 nm and aspect ratio of 13.3 to 5.5 nm (which is calculated from more than 200 nanorods). The F127 addition led to smaller particles with high surface area to volume ratio. Moreover, the pore volume and the metal dispersion of Ni effectively changed and enhanced after F127 incorporation.

The reduced Ni supported Sr-HAP catalysts at 450 °C was investigated by TEM analysis. Figure 3 displayed the TEM images and the corresponding particle size distribution in histograms was presented. The TEM images are clearly presented as the nanorods shaped Sr-HAP particles with different dimensions (Fig. S2). Moreover, Ni particles are highly visible over the nanorod Sr-HAP surface. Furthermore, the F127 mediated sample presented a narrow and homogeneous distribution of Ni particles with average size of ~ 5.7 nm (Fig. 3). Thus, the Ni/Sr-HAP(F127) formed highly homogeneously dispersed Ni particle with smaller size than the bigger Sr-HAP nanorods.

5.3 Surface Area and Particle Size

Both samples exhibited different textural and morphological properties. From Table 1, the F127 co-block polymer

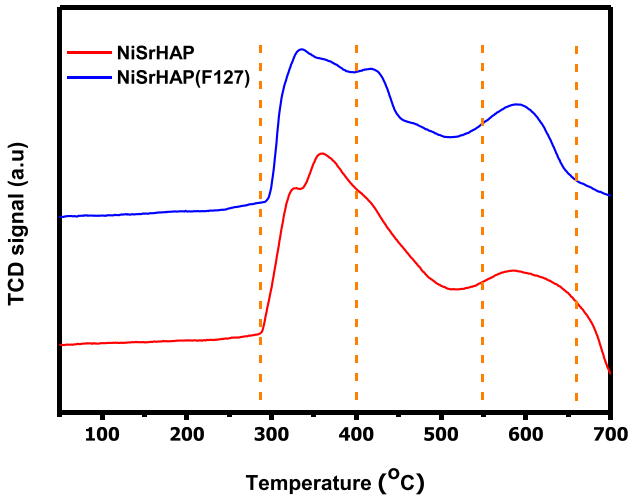

Fig. 4 H_2-TPR analysis of **a** Ni/Sr-HAP and **b** Ni/Sr-HAP(F127) catalysts

mediated Ni/Sr-HAP sample possessed relatively higher and better textural properties in terms of specific surface area, pore size and pore volume than Ni/Sr-HAP. The N_2 adsorption–desorption isotherms presented a characteristic of a mesoporous material. The effect of structure directing agent influenced positively and enhanced surface area due to creation of microporosity. Both samples follow type-II adsorption isotherms with hysteresis loop of H4 (according to IUPAC) with limited amounts of meso-and micropores. After Ni incorporation, the surface area and pore characteristics decreased compared to bare support.

From H_2 chemisorption analysis of Ni/Sr-HAP(F127), the active Ni metal surface area is higher and also exhibited a smaller Ni particle size. Thus, the F127 promoted in converting the bigger nanorod sized Sr-HAP into much smaller active rod-shaped which influenced the dispersion Ni particles narrowly over the HAP.

5.4 TPR and TPD Results

The reducibility profiles of Ni/Sr-HAP catalysts are presented in Fig. 4 and both catalysts exhibited different reducibility behavior (Fig. 4). The surface NiO species are easily reducible to Ni^0 metallic, which are highly dispersed and weakly adsorbed over Sr-HAP surface.

Typically, at low temperatures, decomposition of Ni precursors and hydroxyl groups are reduced at the surface and the remaining –OH groups are the ones strongly bonded and chemisorbed. The reduction profile resulted in five distinctive peaks, in which three peaks are in low temperature region and two peaks were found at high temperature region. The peak regions are designated as weak (below 300 °C), medium (300–400 °C), and strong (above 400 °C) temperature regions of the reduced NiO species with H_2 consumption (Fig. 4). A highly dispersed NiO particles were presented over the HAP surface, which are reduced easily at low to moderate temperature region. First peak at ~ 327 °C Over Ni/Sr-HAP(F127) catalyst, the peaks are broader and a high amount of H_2 is consumed in reducing the surface and sub-surface NiO ($NiO + H_2 -> Ni + H_2O$) including at 358.7 °C and 416 °C. Moreover, above 500 °C the reduction of HAP was initiated and exhibits a broader peak which is assigned to bulk NiO reduction and partial decomposition of strontium phosphate hydrates. Further, the bulk NiO species are reduced at higher temperatures, and which are strongly bonded in the HAP structure. Most of NiO species are fine particles presented over the strontium phosphate hydrate crystal surface. As reported by Steiger et al. the enhanced Ni reducibility and segregation was resulted by

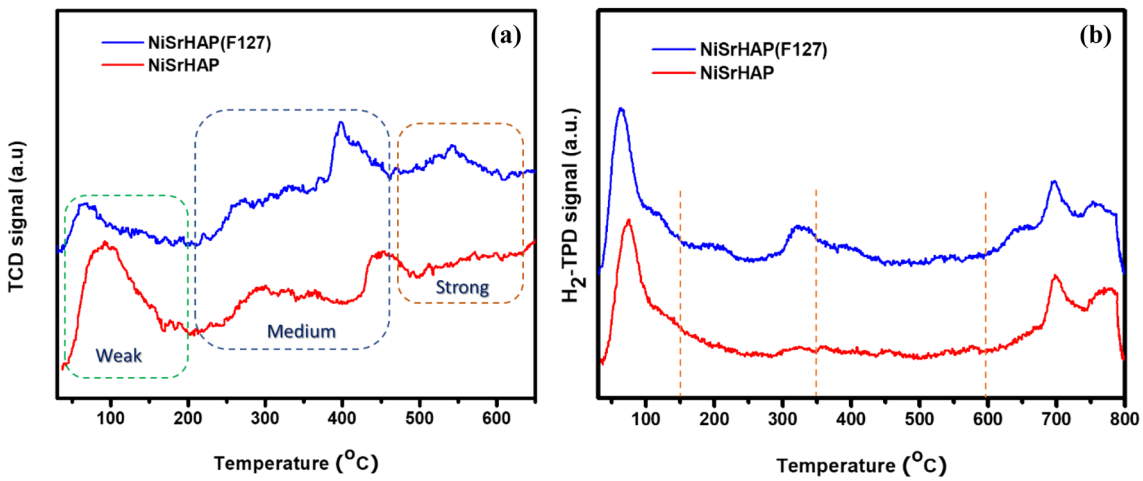

Fig. 5 TPD analysis and the corresponding desorption capacities of **a** CO_2 and **b** H_2 TPD analysis of Ni/Sr-HAP catalysts

Sr incorporation due to Ni exsoluted during pre-reduction. The F127 assisted Ni/Sr-HAP sample exhibited slightly better reducibility behavior at low temperatures than the Ni/Sr-HAP sample and other alkali and alkaline oxides supported catalysts [13, 14].

5.5 CO_2/H_2 Adsorption Capacity Analysis

Basicity measurements of all samples are carried out by CO_2-TPD technique using CO_2/He gas adsorption/desorption conducted from 40 to 650 °C. The temperature programmed desorption of CO_2 and H_2 (CO_2/H_2-TPD) was studied over Ni/Sr-HAP catalysts (Fig. 5a, b). The CO_2 desorption profiles are presented in Fig. 5a and the desorption amounts are recorded on the samples after pre-adsorption of CO_2 at 30 °C for 0.5 h and flushed with He at 110℃. Thus, it is evident that the presence of various adsorption sites exhibiting different thermal stability.

Both Ni/Sr-HAP catalysts exhibited almost similar basicity profiles. However, the strength of adsorption is determining factor in catalyst performance in CO_2/CO methanation. The CO_2 adsorption capacity is reported higher over calcium hydroxyapatite materials than the other alkaline and alkali oxides. Whereas the strontium HAP exhibited slightly higher CO_2 adsorption capacity than Ca-HAP due basic character Silvester et al. [23]. The adsorption of CO_2 preferentially occurs over two basic sites *i.e.,* PO_4^{2-} and surface hydroxyl groups. The strength of basicity is an important property of the solid catalyst surface. The weak basic sites are associated to the surface –OH groups, the medium basic sites are connected to metal–oxygen pairs, and the strong basic sites are related to the low-coordination oxygen anions Ogo et al. [19]. The CO_2 adsorption capacity over two samples is moderately higher than the other alkali and alkaline modified HAP supports.

According to many studies reported, CO_2 desorption strength determined at three different temperature zones and denoted as weak basic sites (around 100–200 °C), moderate basic sites (200–350 °C), and strong basic sites (above 400 °C) [12]. The relatively strong basic sites showed CO_2 desorption above 400 °C, and the weak to medium basic sites presented CO_2 desorption at around 100–350 °C. The CO_2-TPD intensity at around 200–300 °C increased and these medium to weak basic sites play an important role in methanation activity via CO_2 adsorption and C = O activation. The Ni/Sr-HAP possess higher weak basic sites density then the medium and strong basic sites, whereas F127 modified Ni/Sr-HAP exhibited slightly higher amounts of medium basic sites than weak and strong basic sites.

Hydrogen- TPD (H_2-TPD) was analysed, and the desorption profiles were displayed in Fig. 5b. Generally, H_2 adsorbs over the Ni sites and activate the H–H bond scission and finally, spillover effect to the adjacent to $CO_{2,ads}$ over Sr-HAP. Typically, H_2 adsorption over Ni sites takes place well below 200 °C. The H_2 adsorption occurs over Ni surface, subsurface and including the bulk Ni/NiO sites. The desorption profiles of H_2 divided into low temperature zone *i.e.,* the weakly and loosely bonded Ni–H below 200 °C and the moderate H_2 desorption occurs between 200 and 400 °C and the strongly chemisorbed H_2 is typically desorbed at higher temperatures *i.e.,* above 400–500 °C. Nevertheless, the Ni/Sr-HAP prepared with F127 structure directing agent had higher H_2 desorption amounts at moderate temperature range than the simple Ni/Sr-HAP. As predicted that the higher metal surface area of Ni/Sr-HAP(F127) tends to exhibit a higher H_2 adsorption capacity in the optimized reaction temperature wherein, activation of carbonates to form methyl radicals, and furtherto methane formation. As reported, in Sr^{2+} based HAP structure exhibited better solubility than Ca^{2+}-HAP. This phenomenon was confirmed by Christoffersen et al. [28], the solubility of apatite increases with the Sr content.

The Ni/Sr-HAP catalysts comprises different basicity strength and follows the descending order of sites strength: medium > weak > strong. Thus, medium basic sites are dominant in the Ni/Sr-HAP catalysts. In Fig. 6. depicted the most common and plausible acid–base sites and typically weak sites and strong basic sites are those corresponds to –OH groups. Moreover, the anions O^{2-} presented in PO_4^{2-} are the less basic centers than -OH groups.

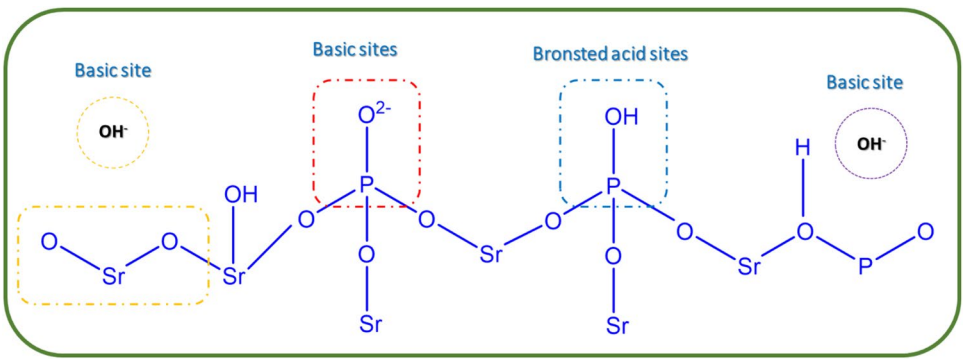

Fig. 6 The depiction of plausible different types of acid–base sites of the Sr-HAP support [21]

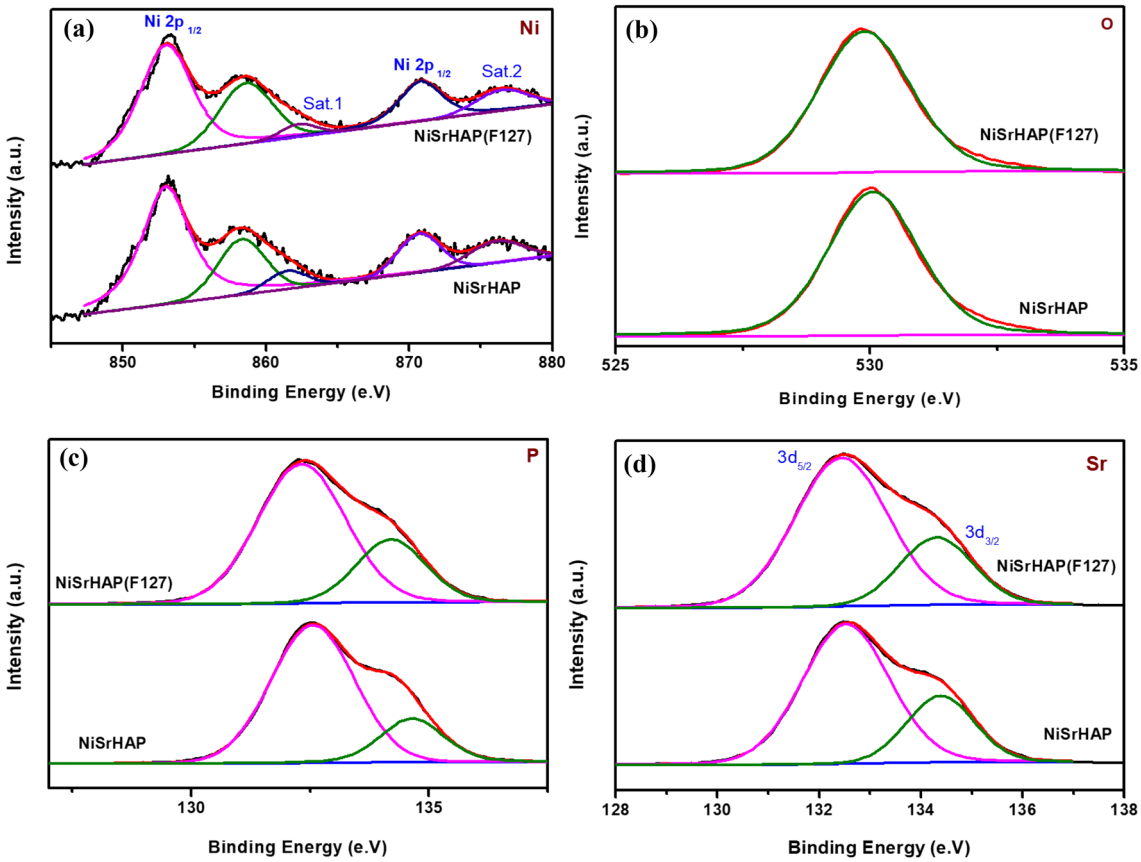

Fig. 7 The XPS spectra of Ni/Sr-HAP and Ni/Sr-HAP(F127) catalysts **a** Ni2p, **b** O1s, **c** P2p, & **d** Sr3d spectras

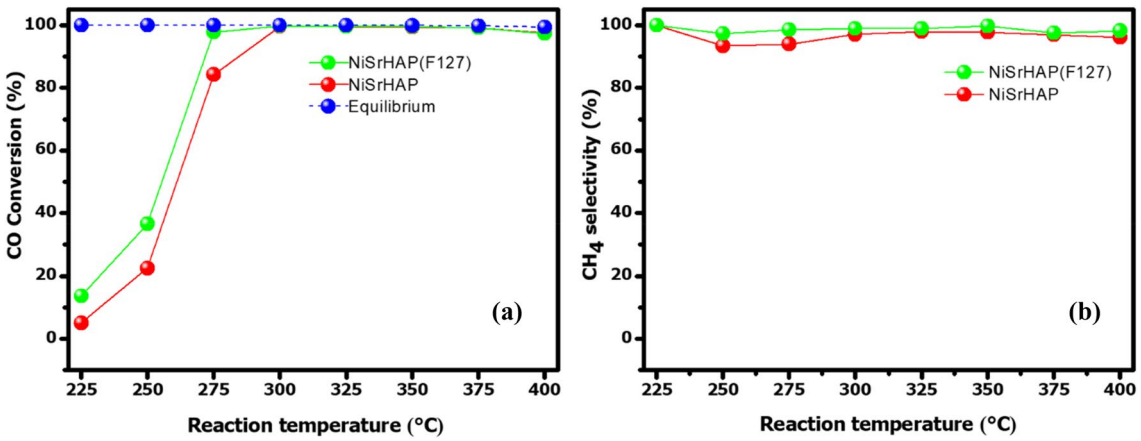

Fig. 8 CO methanation activity results: **a** CO conversion and **b** CH_4 selectivity over synthesised Ni/Sr-HAP and Ni/Sr-HAP(F127) catalysts (reaction conditions: GHSV = 18 000 mL g^{-1} h^{-1}, feed: 20 vol.% CO + 80 vol.% H_2, p = 0.1 MPa)

From elemental analysis (EDX), the Sr/P molar ratio in Ni/Sr-HAP catalysts was found to be ~ 1.5 and at this ratio, possess a relatively high basicity than acidity. In Ogo et al. [19], reported at lower Sr/P ratios (< 1.6), almost very low acid site density was analysed with moderately high basicity was found at 250 °C. Thus, basic sites especially medium to weak strength sites are dominating factors in adsorption and activation of CO_2. The weak and medium

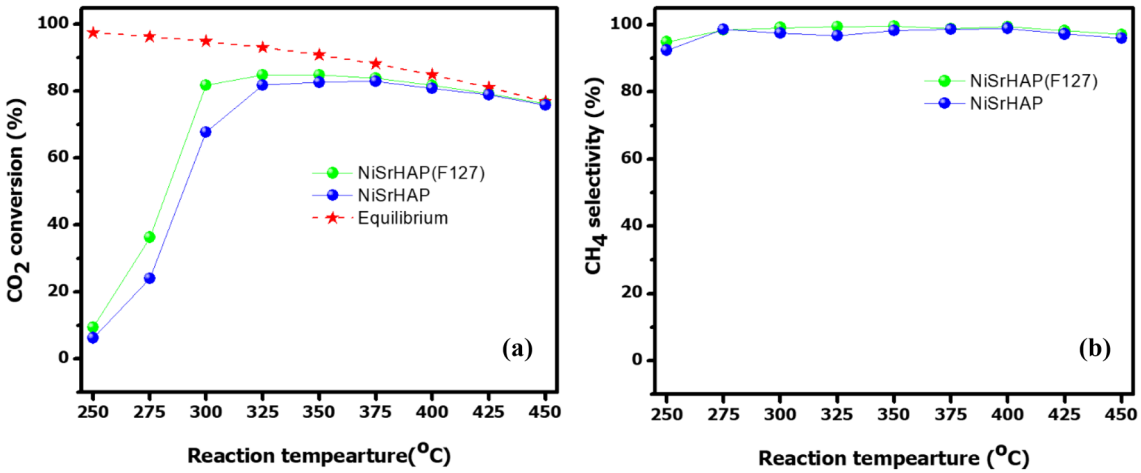

Fig. 9 CO_2 methanation results **a** CO_2 conversion and **b** CH_4 selectivity over the synthesized Ni/Sr-HAP and Ni/Sr-HAP(F127) catalysts (reaction conditions: GHSV = 18 000 mL g^{-1} $h.^{-1}$, feed: 20 vol.% CO_2 + 80 vol.% H_2, p = 0.1 MPa)

basic sites are separately formed by the formation of phosphate anions bonded to Sr^{2+} and SrO species (*i.e.,* O^{2-} anions), while the strongest basic sites are the ones associated with OH^- anions/hydroxyl groups [29].

5.5.1 XPS Results

The elemental composition and surface chemical state of both samples were characterized by XPS measurements after reduction at 450 °C under H_2 flow. The XPS spectrum reveals the similar spectra for both Ni/Sr-HAP catalysts and the spectrum is composed of Ni, O, P and Sr elements; and the Ni content over the surface is about ~ 10 wt.%, which is close to the nominal loading. The existence of Ni and its chemical state can be analysed in high resolution Ni 2p XPS spectrum. The two typical peaks at 852.9 and 870.5 eV can be assigned to Ni 2p3/2 and Ni 2p1/2 peaks, while other two peaks at 861.6 and 876.1 eV are assigned to the satellite peaks. The peak at 858.2 eV B.E is obtained from oxidized state of nickel particles and this NiO presence may be due to the sample transformation for XPS measurements. The O1s spectrum was corresponded to the O^{2-} state which is characterised from the metal-oxide bonding in PO_4^{2-} molecule. Next, the overlapping spectra (P 2p and Sr 3d) was noticed from the Sr-HAP surface due to their proximity and this is well documented with the previously reported studies. Both samples exhibit almost identical spectral data and there is no distinguished chemical state was identified (Fig. 7).

5.6 Catalyst Activity Results of CO/CO_2 Methanation

The CO/CO_2 methanation light-off tests were performed in the temperature range of 225–400 °C (for CO) and 250–450 °C (for CO_2) under ambient pressure (Figs. 8, 9). Pure support Sr-HAP exhibited poor methanation activity in studied temperature range in both methanation reactions compared to Ni/Sr-HAP catalysts. After Ni incorporation, both Ni/Sr-HAP and Ni/Sr-HAP(F127) are highly active and selective in CO/CO_2 methanation. The equilibrium CO/CO_2 conversions (calculated by using Gaseq software) and methane selectivities were compared with the activity results. The CO/CO_2 methanation reactions are exothermic reactions and thermodynamically limited, complete conversion and CH_4 selectivity was achieved at low temperatures. However, at low temperatures arelatively low activity was exhibited due to highly stable CO/CO_2 molecules. Nevertheless, CO and CO_2 conversion increased with reaction temperature to activate the C = O bonds.

Thus, moderate temperatures are needed to achieve the high conversion and selectivity. The CO conversion is stabilized and maintained constant activity above 300 °C and the selectivity remained constant *i.e.,* close to 100%

Table 2 Light-off activity results for CO/CO_2 methanation over various Ni/Sr-HAP catalysts

Reaction	Catalyst	*T_{50}, °C	#T_{80}, °C
CO methanation	Ni/Sr-HAP	265	274
	Ni/Sr-HAP(F127)	252	268
CO_2 methanation	Ni/Sr-HAP	284	350
	Ni/Sr-HAP(F127)	276	296

*T_{50} and #T_{80} light-off temperatures at ~ 50% and ~ 80% conversions

throughout the light-off temperatures. As predicted, the conversion of CO is much faster rate than CO_2 and over Ni/Sr-HAP catalysts, the activity in both methanation reactions is profound and achieved close to equilibrium for above 275 °C in case of CO and above 350 °C for CO_2 conversions. In case CO methanation, a complete conversion was achieved over Ni/Sr-HAP(F127) catalyst at 275 °C and over Ni/Sr-HAP complete conversion obtained at 300 °C. Typically, CO is more easily activated over the catalyst surface and requires low heat of adsorption than CO_2. Whereas, the CO_2 conversion exhibited similar volcano trend, reached maximum conversion of ~ 83% with ~ 98% CH_4 selectivity at 325 °C under ambient pressure and thereafter remained constant until 375 °C. The stochiometric molar ratio is sufficient to achieve high conversions and selectivity close to equilibrium values. Further increase in temperature, the CO_2 conversion declines after 375 °C due to drop in activity to form more CO than CH_4 and this trend is well substantiated with thermodynamical values [30]. Probably the activity loss also due to the reverse water gas shift (RWGS) and disproportionate reactions in the carbon formation, which is typically occurs at high temperatures.

The methane selectivity is almost followed a similar trend in CO/CO_2 methanation i.e., around ~ 95–99% was achieved. The values of CH_4 selectivity is close to equilibrium calculations and a similar selectivity was reported in many studies [12, 14, 30]. In the literature, most of the active and selective Ni-based catalysts had produced similar selectivity values. Thermodynamically, below 250 °C temperature, the equilibrium values close to 100% CH_4 selectivity was achieved. However, the activity results in the current work were gained somewhat better and on par with the published reports above 350 °C (i.e., CO_2 conversion). Summarised the light-off tests results in Table 2 and compared at 50% & 80% CO and CO_2 conversion values (T_{50} & T_{80}).

Over Ni/Sr-HAP(F127) catalyst, the CO and CO_2 conversions at light-off tests produced superior results than Ni/Sr-HAP (Table 2). The ~ 50 and ~ 80% CO_2 conversion was achieved at relatively low temperatures *i.e.,* 276 & 284 °C. Whereas, over Ni/Sr-HAP, the ~ 80% conversion reached at 350 °C, which is much higher temperatures than the T_{80} for Ni/Sr-HAP(F127). The methane production rates were calculated at lower conversion levels. Over Ni/Sr-HAP catalysts, CH_4 production rates are 2.53 and 3.8 mmol g^{-1} s^{-1} at 9.3 and 6.2% CO_2 conversion levels and in the case of CO methanation, a high methane production rates were obtained *e.g.,* 14.9 mmol g^{-1} s^{-1} at 36.5% conversion (see Table S2). These light-off tests results are in good comparison with the published data and in this work, a superior performance was displayed at moderately lower temperatures. Example in Boukha et al. [18], compared the T_{50} with published data and the T_{50} reported temperatures are in range of 300–500 °C, which are relatively higher than the present work.

The correlation of catalytic properties with that of activity results will be discussed. Physicochemical properties such as active metal area, particle size, structure, basicity, and the reducibility etc. are highly crucial in methanation reaction. The prepared Ni/Sr-HAP catalyst with and without F127 was tested and exhibited high activity in both CO/CO_2 conversions and methane selectivity in studied light-off tests (100–450 °C). There is a clear evident that F127 co-block polymer act as a structure directing agent and mediated the growth of Sr-HAP nanorods morphology much smaller size. This phenomena of F127 surfactant significantly improved the physical and chemical properties of the catalyst such as surface area, basicity, and the reducibility Samsudin et al. [31]. Incorporation of F127 is well studied and reported in the materials preparation methods *e.g.,* F127-assisted sol–gel process and moreover, F127 is known for the structure and pore directing group. Pluronic F127 solely effects the final morphology, crystallite size, surface area and microporosity of the carrier materials. Support-F127 material calcination under elevated temperatures, the polymeric organic templated contained composite is readily decomposed and assist in the creation of new porosity to gain high specific area. In this work, it is evident that, Sr-HAP support preparation with F127 addition had increased the surface area and exhibited

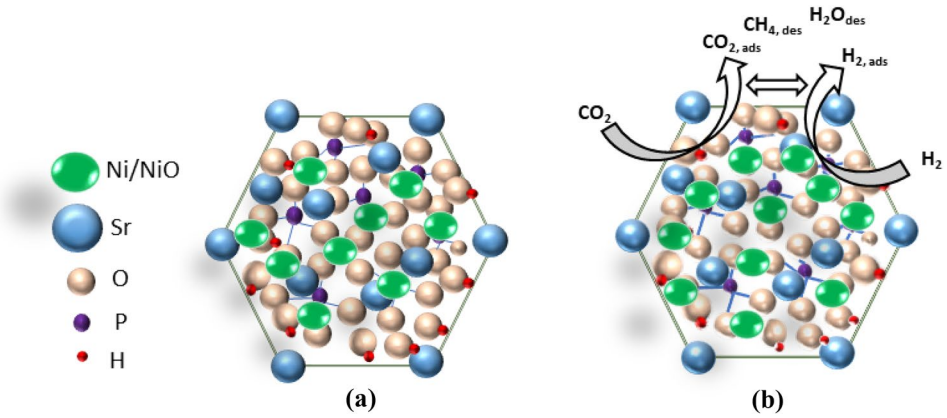

Fig. 10 **a** Illustration of hexagonal crystal structure of strontium phosphate hydroxyapatite and **b** surface methanation reaction of adsorbed $CO_{2,ads}$/$H_{2,ads}$, reactions, and desorbed reaction products $CH_{4,des}$ and steam H_2O_{des} over studied Ni/Sr-HAP catalysts

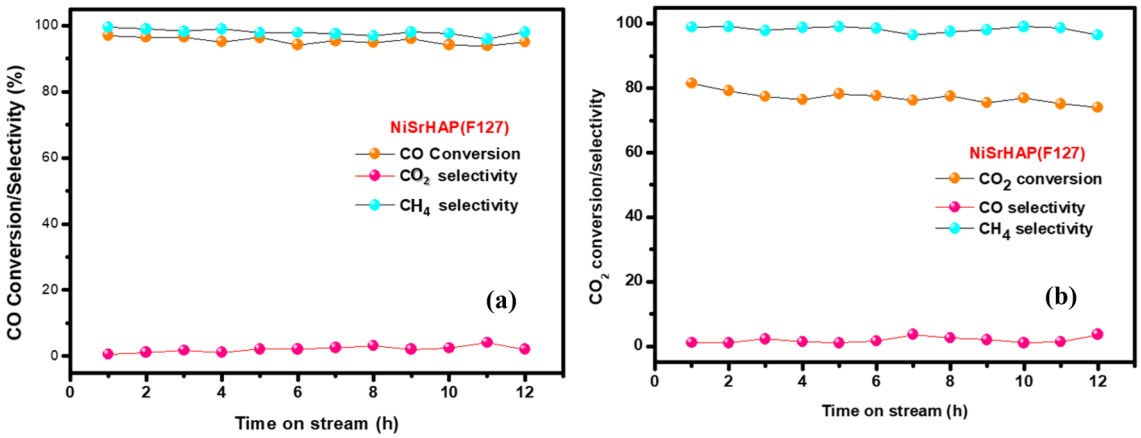

Fig. 11 Time on stream activity testing. **a** CO methanation activity over Ni/Sr-HAP(F127) catalyst (reaction conditions: GHSV = 18,000 mL g^{-1} h^{-1}, T = 275 °C, feed: 20 vol.% CO + 80 vol.% H_2, p = 0.1 MPa). **b** CO_2 methanation activity over Ni/Sr-HAP(F127) catalyst (reaction conditions: GHSV = 18,000 mL g^{-1} h^{-1}, T = 300 °C, feed: 20 vol.% CO_2 + 80 vol.% H_2, p = 0.1 MPa)

higher pore volume. Thus, F127 assisted Sr-HAP support synthesis in Ni catalyst enhanced the catalytic activity. Further, the nanorod shaped Sr-HAP(127) scaffold exhibited much smaller particle size and higher surface-to-volume ratio of strontium phosphates crystals. The F127 assisted in enhancing the Ni dispersion and size in homogeneous distribution over the Sr-HAP surface. This phenomenon had exhibited positive influence in the formation of smaller Ni particle with average size of ~ 5.7 nm. This led the enhanced CO/CO_2 methanation activity at moderately low light-off temperatures (Table 2).

However, the Ni/Sr-HAP catalyst was also shown high activity in carbon oxides conversion and selectivity. At certain light-off temperature, both catalysts shown similar activities. However, at elevated temperatures, F127 assisted Ni/Sr-HAP is more active and selective. A detailed proposed reaction cycle with steps involved in CO_2 adsorption, surface reaction with adjacent spill-over H* from Ni site and desorption of CH_4 and steam was illustrated in Fig. 10. The Ni/Sr-HAP catalysts comprised of metallic Ni^0 sites which are preferable for H_2 adsorption. Typically, CO_2 adsorption take place over basic sites as illustrated in the Fig. 10. As previously reported, Sr-HAP possess high basicity than acidity due to Sr/P molar ratio < 1.6 Silvester et al. [23]. As reported, adsorbed CO_2 forms bicarbonates as intermediate compounds and further decomposed to methyl radical *i.e.,* further hydrogenates to form methane. The Ni/Sr-HAP(F127) was studied in a short time on stream (TOS) test run for a duration of 10–12 test in both CO and CO_2 methanations. From Fig. 11, the catalyst is more stable for first 10 h TOS in CO methanation. Whereas, during CO_2 methanation, the catalysts are stable for initial period of 5–6 h thereafter activity drops due to catalyst deactivation. The CO_2 conversion drops after 6 h and the CO selectivity constant and slight drop in CH_4 selectivity was evident. The carbon formation is negligible at low temperatures due to water formation which suppress the formed carbon. However, the Ni/Sr-HAP(F127) is not stable for long term durability test and the future work will be considered on how to improve the stability of the catalyst for at least over 100 h. A detailed analysis of the used catalysts is highly crucial to know the deactivation phenomena. Typically, in methanation, catalyst deactivation can occur due to Ni sintering, agglomeration, and carbon coke formation covering the active sites (metal sites) or the blocking the pores of the support materials (e.g., re-structuring the basic sites). There are significant structural and morphological changes occur due to deactivation e.g., activity decline owing to inactive sites or no more availability of active metal sites.

It is valid and important to report the state of art on catalysts development for CO_2 methanation in the scientific literature. As we mentioned earlier, majority studies are dedicated to Ni-based catalytic systems and core focus was on the support materials development. Nevertheless, the effect of support materials, additives/promoters, support composition and operating conditions are extensively investigated on Ni-based catalysts and their performance [13]. Recently, one of the approaches in catalyst design and development in the direction for low-temperature methanation. Ni on ceria-based catalysts are applied in low temperature and was found superior due to versatile properties of CeO_2 support such as tunable oxidation state, oxygen mobility, strong metal-support interactions, etc. Varvoutis et al. [31] studied Ni on CeO_2 nanorods with different Ni/Ce ratios and found optimal molar ratio of 1 to gain a 20 nm particle size of Ni found to be most active i.e., 92% CO_2 conversion with 99.7%

Table 3 Comparison of recently reported Ni-based catalysts in the literature with the current work

Catalyst composition (wt.%)	Reaction conditions	X_{CO2} (%)	S_{CH4} (%)	Y_{CH4} (%)	Reference
10% Ni/Sr-HAP(F127)	T = 350 °C; GHSV = 18,000 mL g_{cat}^{-1} h^{-1}; p = 1 bar	83	99	82	This work
15%Ni/H-beta	T = 350 °C; GHSV = 16,000 h^{-1}; H_2/CO_2 = 4; p = 1 bar	80	100	80	[17]
15%Ni Ni/SiO_2	T = 350 °C; GHSV = 16,000 h^{-1}; H_2/CO_2 = 4	70	100	65	[17]
15%Ni Ni/Al_2O_3	T = 350 °C; GHSV = 16,000 h^{-1}; H_2/CO_2 = 4	52	100	40	[17]
3.2%Ni/La_2O_3 (6.6)/HAP	T = 350 oC; GHSV = 30,000 mL g^{-1} h^{-1}; H_2/CO_2 = 4	70	99	70	[18]
30%Ni/Ca-γ-Al_2O_3	T = 300 oC; WHSV = 16,000 mL g_{cat}^{-1} h^{-1}; H_2/CO_2 = 4	93	99	93	[12]
10%Ni/4%SrO/SiO_2	T = 400 °C; GHSV = 15,000 mL g_{cat}^{-1} h^{-1}; H_2/CO_2 = 4	76.3	99	75.5	[22]
Ni/CeO_2-NR	T = 275 °C; WHSV = 30,000 mL g_{cat}^{-1} h^{-1}; H_2/CO_2 = 4	92	99.7	92	[31]
2%Ni@CeO_2-ZrO_2	T = 350 °C; GHSV = 60,000 mL gcat^{-1} h^{-1}; p = 1 bar	58	98	57	[33]
5% Ni/Ca/$Ca_xZr_{1-x}O_{2-\delta}$	T = 350 °C; WHSV = 24,000 mL g_{cat}^{-1} h^{-1}; H_2/CO_2 = 4	72	100	72	[34]
8%Ni/2% CaO/0.8%Ru/Al_2O_3	T = 360 °C; WHSV = 30,000 mLg_{cat}^{-1}.h^{-1}; H_2/CO_2 = 4	80	98	78	[35]
10%Ni/$Ce_{0.9}Ca_{0.1}O_x$	T = 270 °C; WHSV = 36,000 mLg_{cat}^{-1} h^{-1}; H_2/CO_2 = 4	70	95	67	[36]
25%Ni/Y_2O_3	T = 350 °C; WHSV = 36,000 mL g_{cat}^{-1} h^{-1}; H_2/CO_2 = 4	71.5	78	90	[30]
10%Ni/0.5%Ca/30% Ca-TiO_3/Al_2O_3	T = 350 °C; GHSV = 5 000 h^{-1}; H_2/CO_2 = 4	55	100	55	[36]

methane selectivity was achieved at 275 °C with high CH_4 production rate [31]. However, the Ni loading is quite high as 23.5 wt.% and in this work we used only 10 wt.% Ni. The effect of Ni loadings had profound influence on the methanation activity and many reported on finding the most optimal Ni loading in combination with the support structure. Three different of supports are investigated by varying the Ni loadings (5–25 wt.%) over CeO_2, Y_2O_3, Al_2O_3 oxides and the nature of metal-support interactions is a crucial factor in promoting the CO and CO_2 methanation activity. Overall, Ni/Y_2O_3 was the most active and stable catalyst without deactivation in long-term durability test [30]. Thus, support structure and its surface properties are vital in gaining the highest methanation activity. In Guo et al. [22], studied the effect of alkaline metal oxides (MO = Ca, Mg, Sr, Ba) doping in Ni/SiO_2 catalysts. The SrO modified Ni/SiO_2 catalyst enhanced the activity and stability by avoiding the Ni sintering, whereas other oxides exhibited low activity or stability. In Boukha et al. [18] studied the effect of Ni/La ratio in Ni/La-HAP catalysts and the activity in descending order was resulted: Ni/La-(6.6)/HAP > Ni/La-(3.7) /HAP > Ni/La-(1) /HAP > Ni/HAP with T_{50} at 318 °C was achieved (in this work T_{50} at 276 °C, which is significantly lower temperature). As predicted, Ni/Ca-HAP exhibited very low activity in the literature and in this work, the novel Ni/Sr-HAP catalysts produced better activity results in CO/CO_2 methanation reactions due to assisted F127 agent in enhancing the key properties and this similar phenomena by F127 mediated reaction is reported in [32]. We compared our work with some of the most recent results published in the literature on Ni-based catalysts for CO_2 methanation (Table 3).

6 Conclusion

In this work, we prepared a novel Ni impregnated strontium hydroxyapatite (Ni/Sr-HAP) based catalysts. First, two catalyst supports were prepared *i.e.,* one with F127 co-block polymer surfactant which is mediated in the growth of smaller nanorod shaped Sr-HAP and one without F127. The influence of surfactant assisted catalyst preparation had significant effect on the physicochemical properties and the activity. The catalyst structure–activity is well correlated in the CO/CO_2 methanation reactions. Both Ni-based catalysts exhibited high activity in the light-off tests results. The F127 assisted Ni/Sr-HAP(F127) catalyst enhanced the activity and selectivity in CO/CO_2 methanation due to high metal surface area, smaller Ni particle size and optimal properties. Moreover, the F127 assisted catalyst improved the Ni dispersion and reduced the particle size. The Ni/Sr-HAP(F127) catalyst possessed slightly better catalytic properties in terms of reducibility of NiO species at lower temperatures and higher medium to weak basic sites strength. The reaction temperature had profound influence on the activity and the results on CO/CO_2 conversions and selectivity are close to equilibrium values. However, the conversion of CO_2 drops after 375 °C and this phenomenon is well correlated with thermodynamic values. The complete CO conversion was achieved with almost 100% CH_4 selectivity and gained 20 µmol g^{-1} s^{-1} of CH_4 at 250 °C. In case CO_2 methanation, over Ni/Sr-HAP(F127) the light-off activity had superior performance at low temperature than Ni/Sr-HAP. A schematic representation of plausible steps involved in the methanation activity was summarised. Further studies will be conducted to design and develop the Ni/Sr-HAP(F127) catalyst to exhibit high stability and high conversion at relatively low temperatures

without activity loss by addition of promoters and suitable absorbents to shift the thermodynamic limitations.

Supplementary Information The online version contains supplementary material available at https://doi.org/10.1007/s11244-023-01823-6.

Acknowledgements This research was supported by Chungnam National University (2021-2022) and Hycat3 project, University of Oulu.

Funding Open Access funding provided by University of Oulu including Oulu University Hospital. Funding was provided by Hycat3 and Hycamite Oy. This work was also supported by research fund of Chungnam National University.

References

1. Friedlingstein P, Andrew RM, Rogelj J, Peters GP, Canadell JG, Knutti R, Luderer G, Raupach MR, Schaeffer M, van Vuuren DP, Le Quere C (2014) Persistent growth of CO2 emissions and implications for reaching climate targets. Nat Geosci 7:709–715
2. Arakawa H, Aresta M, Armor JN, Barteau MA, Beckman EJ, Bell AT, Bercaw JE, Creutz C, Dinjus E, Dixon DA (2001) Catalysis research of relevance to carbon management: progress, challenges, and opportunities. Chem Rev 101:953–996
3. Wesselink B, Harmsen R, Eichhammer W (2020) Energy savings 2020: how to triple the impact of energy saving policies in Europe Contribut. Stud Roadmap 2050:1–2
4. Schaaf T, Grünig J, Schuster M et al (2014) Methanation of CO2—storage of renewable energy in a gas distribution system. Energ Sustain Soc 4:2. https://doi.org/10.1186/s13705-014-0029-1
5. Mebrahtu C, Krebs F, Abate S, Perathoner S, Centi G, Palkovits R (2019) Chapter 5—CO2 methanation: principles and challenges. In: Albonetti S, Perathoner S, Quadrelli EA (eds) Studies in surface science and catalysis. Elsevier, pp 85–103
6. Hervy M, Maistrello J, Brito L, Rizand M, Basset E, Kara Y, Maheut M (2021) Power-to-gas: CO2 methanation in a catalytic fluidized bed reactor at demonstration scale, experimental results and simulation. J CO2 Utilization 50:101610
7. Boll W, Hochges G, Müller WD (2006) Methanation and methane synthesis Ullmann's encyclopedia of industrial chemistry. Wiley, Weinheim, p 85
8. Schmider D, Maier L, Deutschmann O (2021) Reaction kinetics of CO and CO_2 methanation over nickel. Ind Eng Chem Res 60:5792–5805. https://doi.org/10.1021/acs.iecr.1c00389
9. Ashok J, Pati S, Hongmanorom P, Tianxi Z, Junmei C, Kawi S (2020) A review of recent catalyst advances in CO2 methanation processes. Catal Today 356:471–489
10. Zhao K, Li Z, Bian L (2016) CO2 methanation and co-methanation of CO and CO2 over Mn-promoted Ni/Al2O3 catalysts Front. Chem Sci Eng 10:273–280
11. Falbo L, Visconti CG, Lietti L, Szanyi J (2019) The effect of CO on CO2 methanation over Ru/Al2O3 catalysts: a combined steady-state reactivity and transient DRIFT spectroscopy study. Appl Catal B Environ 256:117791
12. Cho EH, Park YK, Park KY, Song D, Koo KY, Jung U, Yoon WR, Ko CH (2022) Simultaneous impregnation of Ni and an additive via one-step melt-infiltration: Effect of alkaline-earth metal (Ca, Mg, Sr, and Ba) addition on Ni/γ-Al2O3 for CO2 methanation. Chem Eng J 428:131393
13. Ridzuan M, Shaharun MS, Anawar MA, Ud-Din I (2022) Ni-based catalyst for carbon dioxide methanation: a review on performance and progress. Catalysts 12:469. https://doi.org/10.3390/catal12050469
14. Frontera P, Macario A, Ferraro M, Antonucci P (2017) Supported catalysts for CO2 methanation: a review. Catalysts 7:59. https://doi.org/10.3390/catal7020059
15. Kuznecova I, Gusca J (2017) Property based ranking of CO and CO2 methanation catalysts. Energy Proc 128:255–260
16. Lu X, Gu F, Liu Q, Gao J, Liu Y, Li H, Jia L, Xu G, Zhong Z, Su F (2015) VO_x promoted Ni catalysts supported on the modified bentonite for CO and CO2 methanation. Fuel Process Technol 135:34–46. https://doi.org/10.1016/j.fuproc.2014.10.009
17. Liang C, Zhang L, Zheng Y, Zhang S, Liu Q, Gao G, Dong D, Wang Y, Xu L, Hu X (2020) Methanation of CO2 over nickel catalysts: impacts of acidic/basic sites on formation of the reaction intermediates. Fuel 262:116521
18. Boukha Z, Bermejo-López A, Pereda-Ayo B, González-Marcos JA, González-Velasco JR (2022) Study on the promotional effect of lanthana addition on the performance of hydroxyapatite-supported Ni catalysts for the CO2 methanation reaction. Appl Catal Environ 314:121500
19. Ogo S, Onda A, Iwasa Y, Hara K, Fukuoka A, Yanagisawa K (2012) 1-Butanol synthesis from ethanol over strontium phosphate hydroxyapatite catalysts with various Sr/P ratios. J Catal 296:24–30
20. Sugiyama JB (2002) Catal Lett 81:77
21. Ogo S, Onda A, Yanagisawa K (2008) Appl Catal A 348:129
22. Guo M, Lu G (2014) The difference of roles of alkaline-earth metal oxides on silica-supported nickel catalysts for CO2 methanation. RSC Adv 4(102):58171–58177
23. Silvester L, Lamonier JF, Lamonier C, Capron M, Vannier RN, Mamede AS, Dumeignil F (2017) ChemCatChem 9:2250
24. Kim T, Park B (2005) Synthesis and growth mechanisms of one-dimensional strontium hydroxyapatite nanostructures. Inorg Chem 44:9895–9901
25. Lee SJ, Jun JH, Lee SH, Yoon KJ, Lim TH, Nam SW, Hong S (2002) Partial oxidation of methane over nickel-added strontium phosphate. App Catal. A 230:61–71
26. Iqbal MZ, Khan A, Numan A, Alzaid M, Iqbal J (2020) Facile sonochemical synthesis of strontium phosphate based materials for potential application in supercapattery devices. Int J Hydrogen Energy 45:32331–32342
27. Jun JH, Lee SJ, Lee SH et al (2003) Characterization of a nickel-strontium phosphate catalyst for partial oxidation of methane. Korean J Chem Eng 20:829–834. https://doi.org/10.1007/BF02697283
28. Christoffersen J, Christoffersen MR, Kolthoff N, Barenholdt O (1997) Effects of strontium ions on growth and dissolution of hydroxyapatite and on bone mineral detection. Bone 20(1):47–54. https://doi.org/10.1016/S8756-3282(96)00316-X
29. Li D et al (2022) Green Energy Environ 7:691–770

30. Italiano C, Llorca J, Pino L, Ferraro M, Antonucci V, Vita A (2020) CO and CO2 methanation over Ni catalysts supported on CeO_2, Al_2O_3 and Y_2O_3 oxides. Appl Catal Environ 264:118494
31. Samsudin EM, Hamid SBA, Juan JC, Basirun WJ (2015) Influence of triblock copolymer (pluronic F127) on enhancing the physicochemical properties and photocatalytic response of mesoporous TiO2. Appl Surf Sci 355:959–968
32. Vrijburg WL, van Helden JWA, Parastaev A, Groeneveld E, Pidko EA, Hensen EJM (2019) Ceria–zirconia encapsulated Ni nanoparticles for CO2 methanation. Catal Sci Technol 9:5001–5010
33. Everett OE, Zonetti PC, Alves OC, de Avillez RR, Appel LG (2020) The role of oxygen vacancies in the CO2 methanation employing Ni/ZrO2 doped with Ca. Int J Hydrogen Energy 45:6352–6359. https://doi.org/10.1016/j.ijhydene.2019.12.140
34. Liu K, Xu X, Xu J, Fang X, Liu L, Wang X (2020) The distributions of alkaline earth metal oxides and their promotional effects on Ni/CeO2 for CO2 methanation. J CO2 Util 38:113–124. https://doi.org/10.1016/j.jcou.2020.01.016
35. Do JY, Park NK, Seo DW, Lee D, Ryu HJ, Kang M (2020) Effective thermocatalytic carbon dioxide methanation on Ca-inserted NiTiO3 perovskite. Fuel 271:117624. https://doi.org/10.1016/j.fuel.2020.117624
36. Liu Q, Wang S, Zhao G, Yang H, Yuan M, An X, Zhou H, Qiao Y, Tian Y (2018) CO2 methanation over ordered mesoporous NiRu-doped CaO-Al2O3 nanocomposites with enhanced catalytic performance. Int J Hydrogen Energy 43:239–250. https://doi.org/10.1016/j.ijhydene.2017.11.052